considering the C–O bond dipole. (Meta protonation is much less probable due to the less favorable resonance interactions.) We have no way of distinguishing these at present, but isotope effect studies may make this possible. Also, Scheme III shows S_N2 attack by water on the methoxy carbon to give the product, whereas Scheme II shows water addition at the ipso carbon as in Scheme I, which has precedent.[38] These two possibilities are in principle distinguishable by ^{18}O-exchange studies; S_N2 attack should not lead to exchange, whereas water addition would.[8] As well, the mechanisms proposed in Schemes II and III could be tested by carrying out an experiment in D_2SO_4/D_2O, which would lead to incorporation of deuterium on the ring but not in the starting material if either of these schemes is correct. Such experiments are under consideration.

Rate comparisons of the two reactions are probably best made in the standard state, water, and the necessary rate constants can be obtained from the intercepts quoted above. In this medium, the 4-OMe hydrolyzes some 7000 times faster than the 3-OMe and by a totally different mechanism.

The foregoing analysis of the rate data clearly shows that, although the gross kinetic features for the hydrolysis of the two methoxy groups in **1**, as demonstrated by the rate constant/percent H_2SO_4 profiles, are similar, their mechanisms of hydrolysis are fundamentally different. Protonation of the azo group activates the 4-OMe toward attack by nucleophilic water (Scheme I). The downturn in rate which is evident in Figure 1 and persists in Figure 2 is a clear manifestation of the depletion of nucleophilic water at higher acidities,[41] reflected in quantitative (thermodynamic) terms by decreasing a_{H_2O}. An interesting feature of this mechanism is the sensitivity of the k_1 and k_2 steps to water availability due to differential demands for solvation. This is a consequence of the involvement of three water molecules in this S_NAr-type reaction, each water molecule being assigned an active role in the bond making/breaking process.

By contrast, the rate-limiting step in the reaction of the 3-OMe group is ring carbon protonation. Since water is involved *after* the slow step of the reaction, the plot in Figure 2 remains linear across the entire range of acidity investigated, once the fraction of the substrate protonated on the azo nitrogen is accounted for. The downturn in the rate of the reaction of the 3-OMe group (Figure 1) is therefore a result of the protonation of the azo nitrogen, which is preferred over carbon protonation on the grounds of basicity, and converts the substrate into an unreactive form. The apparent similarity of the reaction profiles in Figure 1 is hence illusory. Clearly the existence of this totally different mechanism reflects the fact that the 3-OMe is *not* activated by the protonated azo function; however, it does represent a viable pathway for the hydrolysis of such aromatic substrates in moderately concentrated acidic solutions.

The unravelling of these different pathways and the clear demonstration of a dichotomy in the mode of response of the two reacting methoxy functions to increasing acidity both commend the excess acidity method as a diagnostic tool for studying reaction mechanisms in concentrated acid.

Acknowledgment. We thank the Natural Sciences and Engineering Research Council of Canada for a grant in aid of this research (E.B.) and the Canadian International Development Agency for a visiting fellowship (I.O.). Valuable discussions with Professors A. J. Kresge and Ross Stewart are also acknowledged, as is assistance by S. Poppat with some of the experiments.

Registry No. **1**, 138151-54-9; **4**, 138151-55-0.

Supplementary Material Available: Tables of absorbance data as a function of acidity for **2** (Table SII) and of rate constants as a function of acidity for the hydrolyses of the 4-OMe group of **1** and the 3-OMe group of **2** (Tables SIII and SIV) (3 pages). Ordering information is given on any current masthead page.

(41) Cox, R. A. *J. Am. Chem. Soc.* **1974**, *96*, 1059.

Chemical Trapping of Electronically Excited Biradicals upon Visible Light-Induced Oxygen-Atom Transfer from NO_2 to Allene and Dimethylacetylene in a Cryogenic Matrix

Munetaka Nakata† and Heinz Frei*

Contribution from the Chemical Biodynamics Division, Lawrence Berkeley Laboratory, University of California, Berkeley, California 94720. *Received May 28, 1991. Revised Manuscript Received October 11, 1991*

Abstract: Oxygen-atom transfer from NO_2 to allene and dimethylacetylene was observed upon excitation of reactant pairs in solid Ar at wavelengths as long as 585 (NO_2 + allene) and 610 nm (NO_2 + dimethylacetylene). Continuous wave dye laser radiation was used to initiate reaction, and product growth was monitored by FT-infrared spectroscopy. In the case of the allene + NO_2 reaction 2-allyl nitrite radical was obtained as product, while excitation of dimethylacetylene–NO_2 pairs gave acetyl methyl iminoxy radical and dimethylketene + NO. Structures of products were determined by ^{15}N and ^{18}O isotopic substitution and, in the case of allyl nitrite radical, by observation of photodissociation products allene oxide and cyclopropanone. The observed radicals constitute transient biradicals formed upon O-atom transfer that are chemically trapped by NO cage coproduct. Interpretation by aid of literature ab initio results indicates that in the case of allene + NO_2 the observed nitrite radical is 2-allenylidoxy biradical trapped in a B_1 excited state. The iminoxy radical product of the dimethylacetylene photooxidation is a trapped singlet excited acetylmethyl methylene biradical. This is the first insight into O-atom transfer paths involving cumulene and CC triple bonds gained by chemical trapping of excited-state biradicals.

I. Introduction

Knowledge of detailed oxidation paths of small unsaturated hydrocarbons is of strong current interest in the area of product-specific conversion of these abundant chemicals to high-valued compounds.[1] Oxidation mechanisms of unsaturated hydrocarbons are of equal importance in combustion[2] and atmospheric chem-

† Present address: Tokyo University of Agriculture and Technology, 3-5-8 Saiwai-cho, Fuchu, Tokyo 183, Japan.

(1) Szmant, H. H. *Organic Building Blocks of the Chemical Industry*; Wiley: New York, 1989.

0002-7863/92/1514-1363$03.00/0

istry.[3] In the case of alkyne oxidations in solution, product distributions observed with commonly used peroxy acids have occasionally led to the postulation of oxirene as intermediate.[4,5] However, the controversy about intermediacy of this species and proposed alternatives like ketocarbene or oxirene biradicals[2,4,5] that may be formed along the reaction path remains unresolved since no such species have yet been observed upon O-atom transfer to CC triple bonds. On the other hand, detailed dynamical information on the prototype $O(^3P)$ + HC≡CH reaction obtained by Lee and co-workers in crossed molecular beam experiments revealed that this reaction proceeds primarily on the triplet ground-state surface of HCC(O)H biradical intermediate[6] in agreement with previous theoretical work by Harding and Wagner based on ab initio calculations.[7] Similarly, no transients have hitherto been detected in the case of allene oxidations,[8] but Lee has determined the branching between central vs terminal carbon attack in the case of the $O(^3P)$ + CH_2=C=CH_2 reaction by a crossed molecular beam study under single collision conditions.[9] Previous ab initio work on the potential energy surface of this reaction by Lester and co-workers reported energies of triplet ground-state 2-allenylidoxy and 1-allenylidoxy biradical intermediates proposed to be formed upon central and terminal atom attack, respectively.[11] Products observed by Singmaster and Pimentel upon red light induced O-atom transfer of ozone–allene complexes in rare gas matrices also signal reaction at both the central and terminal carbons.[12] Allene oxide was detected for the first time, but no reaction intermediate was trapped.

We have recently found that oxygen-atom transfer from long wavelength visible light excited NO_2 to small olefins in a solid rare gas matrix results in formation of epoxides as the sole final oxidation products with high stereochemical integrity.[13-18] In the case of terminal CC bonds aldehydes were also produced.[15,16] Concurrently, alkyl nitrite radicals were detected. Correlation of the stereochemistry of nitrite radical and final oxidation products and wavelength-dependent photolysis studies revealed that the observed nitrite radicals originate from transient oxirane biradicals that are chemically trapped in their nascent conformation by combination with NO coproduct.[13-15] Hence, large amplitude oxygen-atom transfer[17] of NO_2–alkene collisional pairs (vibronic excitation of NO_2 well below the 398-nm dissociation limit to $O(^3P)$ + NO) yields biradicals which either are stabilized by ring closure (or by 1,2-H shift) to give a stable oxidation product or combine with NO while retaining the initial conformation. This allowed us to determine detailed stereochemical paths of ethylene,[15] *cis*- and *trans*-2-butene,[13,14] isobutylene,[16] cyclopentene, and cyclohexene oxidation.[17]

We have explored the method of visible light induced O-atom transfer of NO_2–hydrocarbon pairs in a rare gas matrix for elucidation of the detailed paths of cumulene and triple-bond oxidation by attempting to trap nascent states of transient biradicals. Since according to the conservation of spin rule not only triplet but also singlet biradicals may emerge upon O-atom transfer from NO_2, these experiments opened up the possibility of uncovering the detailed reaction path operative upon oxidation of allene or alkyne by common closed shell oxygen donors like peroxy acids.

In this paper, we report our results on long wavelength visible light initiated oxidation of allene and dimethylacetylene by NO_2. Wavelength-dependent photochemistry of allene–NO_2 and dimethylacetylene–NO_2 pairs isolated in solid Ar at 12 K was conducted with tuned continuous wave dye laser radiation and the chemistry monitored by Fourier transform infrared spectroscopy.

II. Experimental Section

Matrix suspensions of allene and NO_2 or dimethylacetylene and NO_2 in solid Ar were prepared by slow continuous deposition of gas mixtures onto a 12 K cooled CsI window. Details of the technique are described in ref 13. Concentration ratios used were hydrocarbon/NO_2/Ar = 2.5/1/100, 2.5/1/200, and 2.5/1/400. Chemical reaction was monitored by infrared spectroscopy using an IBM-Bruker Model 97 FT-IR spectrometer at 0.5-cm^{-1} resolution. For laser irradiation with a prism tuned Ar ion laser or an Ar ion laser pumped CW dye laser (Coherent Innova Models 90-6 and 599-01), the 12 K cooled CsI window was rotated 90° to expose the matrix to photolysis light entering the vacuum shroud of the cryostat (Air Products Displex Model CSA 202) through a quartz window. Laser power was monitored before and after each irradiation period using a Coherent Model 210 power meter. Measurements were made directly in front of the quartz entrance window. Photolysis (266 nm) of diacetyl monoxime was performed with the fourth harmonic of a pulsed (5 ns, 10 Hz) Nd:YAG laser (Quanta Ray Model DCR-2A).

Allene (Matheson), allene-d_4 (MSD Isotopes, 99.3%), dimethylacetylene (API, Carnegie Institute of Technology, 99.93%), and 2,3-butanedione monoxime (Aldrich, 97%) were used as received. NO impurity was removed from NO_2 (Matheson, 99.5%) as described in previous work.[13] $^{15}NO_2$ (Icon Services, Inc., 99 atom % ^{15}N) was purified by LN_2 trap to trap distillation before use. Two samples of ^{18}O containing nitrogen dioxide were prepared by gas-phase oxidation of $N^{18}O$ (Icon Services, 94.5%) by oxygen. When $^{18}O_2$ (MSD Isotopes, 98.2%) was used, a sample containing 94% $N^{18}O_2$ was obtained. When $^{16}O_2$ was used, the resulting mixture was $N^{16}O_2/N^{16}O^{18}O/N^{18}O_2$ = 1/2/1. Argon (Matheson, 99.998%) was used without further purification.

III. Results

1. Allene + NO_2. We will first present infrared spectral data that allowed us to identify the products of the visible light induced allene + NO_2 reaction. Then, the photolysis wavelength dependence of the product growth kinetics will be discussed.

1.1. Infrared Spectra. Since no infrared product growth has been observed at frequencies above 2200 cm^{-1}, we will confine the report of infrared data to the region 2200–400 cm^{-1}. Upon deposition of matrices $C_3H_4/NO_2/Ar$ = 2.5/1/200, C_3H_4 bands were found at 1999, 1956, 1945, 1910, 1680, 1437, 1390, 1353, 1194, 1071, 1025, 997, 865, 854, and 838 cm^{-1},[19] while NO_2 absorbed at 1609 cm^{-1} [20] ($^{15}NO_2$, 1577 cm^{-1}; $N^{16}O^{18}O$, 1593 cm^{-1}; $N^{18}O_2$, 1581 cm^{-1}). N_2O_4 isomers, together with traces of N_2O_3 impurity, were also trapped. The infrared spectra of these species and their photoisomerization behavior under irradiation with red light have been summarized in Table I of ref 13 (see ref 21 for corresponding data on $^{15}N_xO_y$ and $N_x{}^{18}O_y$). Allene-d_4 in matrices $C_3D_4/NO_2/Ar$ = 2.5/1/200 showed bands at 2197, 1930, 1918, 1911, 1895, 1871, 1643, 1339, 1166, 1146, 1132, 1106, 1102, 1078, 1073, 1028, 970, 823, 796, 713, 671, 664, 654, and 532 cm^{-1}.[22] No infrared absorptions of allene–NO_2 nearest neighbors separate from those of isolated reactants were found.

The longest wavelength at which photochemistry of allene–NO_2 pairs could be detected was 585 nm. To minimize interferences from infrared spectral changes originating from N_xO_y photoisomerization, allene/NO_2/Ar matrices were irradiated with

(2) Hucknall, D. J. *Chemistry of Hydrocarbon Combustion*; Chapman and Hall: London, 1985.
(3) Wayne, R. P. *Chemistry of Atmospheres*, 2nd ed.; Oxford University Press: Oxford, U.K., 1991.
(4) Lewars, E. G. *Chem. Rev.* **1983**, *83*, 520–34. Early work on the mechanism of alkyne oxidations has been reviewed in this paper and in refs 2 and 5.
(5) Torres, M.; Lown, E. M.; Gunning, H. E.; Strausz, O. P. *Pure Appl. Chem.* **1980**, *52*, 1623–43.
(6) Schmoltner, A. M.; Chu, P. M.; Lee, Y. T. *J. Chem. Phys.* **1989**, *91*, 5365–73. For earlier gas-phase work on $O(^3P)$ + acetylene reaction see references cited therein.
(7) Harding, L. B.; Wagner, A. F. *J. Phys. Chem.* **1986**, *90*, 2974–87. Michael, J. V.; Wagner, A. F. *J. Phys. Chem.* **1990**, *94*, 2453–64.
(8) Chan, T. H.; Ong, B. S. *J. Org. Chem.* **1978**, *43*, 2994–3001.
(9) Schmoltner, A. M.; Huang, S. Y.; Brudzynski, R. J.; Chu, P. M.; Lee, Y. T. Submitted for publication. For earlier gas-phase work on $O(^3P)$ + allene see ref 10 and references cited therein. We thank Professor Lee for a preprint of this work.
(10) Aleksandrov, E. N.; Arutynnov, V. S.; Kozlov, N. *Kinet. Katal.* **1980**, *21*, 1327–34.
(11) Hammond, B. L.; Huang, S.-Y.; Lester, W. A., Jr. *J. Phys. Chem.* **1990**, *94*, 7969–72.
(12) Singmaster, K. A.; Pimentel, G. C. *J. Mol. Struct.* **1989**, *194*, 215–38.
(13) Nakata, M.; Frei, H. *J. Am. Chem. Soc.* **1989**, *111*, 5240–7.
(14) Nakata, M.; Frei, H. *J. Phys. Chem.* **1989**, *93*, 7670–7.
(15) Nakata, M.; Shibuya, K.; Frei, H. *J. Phys. Chem.* **1990**, *94*, 8168–75.
(16) Nakata, M.; Frei, H. *J. Chem. Soc. Jpn.* **1989**, 1412–7.
(17) Fitzmaurice, D. J.; Frei, H. *J. Phys. Chem.* **1991**, *95*, 2652–61.
(18) Frei, H. *Chimia* **1991**, *45*, 175–90.
(19) Jacox, M. E.; Milligan, D. E. *Chem. Phys.* **1974**, *4*, 45–54.
(20) Fateley, W. G.; Bent, H. A.; Crawford, B., Jr. *J. Chem. Phys.* **1959**, *31*, 204–17.
(21) Harrison, J. A., Frei, H. Unpublished results.
(22) Lord, R. C.; Venkateswarlu, P. *J. Chem. Phys.* **1952**, *20*, 1237–47.

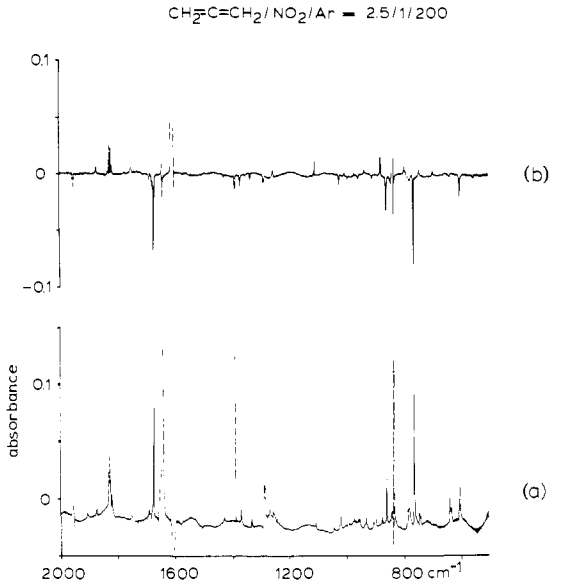

Figure 1. (a) Infrared difference spectrum obtained upon irradiation of a matrix allene/NO_2/Ar = 2.5/1/200 at 580 nm for 4 h (490 mW cm^{-2}). Dashed lines indicate N_xO_y and reactant absorptions; (b) infrared difference spectrum obtained upon 6-min photolysis of matrix a at 488 nm (80 mW cm^{-2}).

Table I. Infrared Spectrum of Trapped Nitrite Radical in a Matrix Allene/NO_2/Ar = 2.5/1/200 (Frequency, cm^{-1})

C_3H_4ONO[a]	$C_3H_4O^{15}NO$	C_3D_4ONO
1673.7 (1.00)	1644.5	1673.7
1429.0 (0.03)	1429.0	1116.6
1370.6 (0.14)	1370.5	1014.5
1334.8 (0.08)	1334.1	995.0
1023.6[b]	1021.0	908.0
957.7 (0.06)	956.1	844.6
862.8 (0.45)	862.8	838.9
765.7 (1.18)	755.7	742.6
605.0 (0.29)	602.0	685.0

[a] In parentheses: relative (peak) absorbances, normalized with respect to the absorbance of the 1674-cm^{-1} band. [b] Band overlaps with allene absorption.

620-nm light for 1–2 h at 400 mW cm^{-2} immediately after deposition. Only small intensity changes occurred among N_xO_y species when the photolysis laser was subsequently tuned to wavelengths shorter than the 585-nm allene + NO_2 reaction threshold. Figure 1a displays the infrared product growth in the range 2200–400 cm^{-1} upon 4 h of irradiation of a matrix C_3H_4/NO_2/Ar = 2.5/1/200 at 580 nm (490 mW cm^{-2}). The three most intense product bands observed are at 1673.7, 862.8, and 765.7 cm^{-1}. These absorptions exhibit identical growth kinetics, which was found to be linear in photolysis light intensity. The additional weaker product bands fall into three categories according to their behavior upon photolysis at a number of different wavelengths. Bands at 1429.0, 1370.6, 1334.8, 1023.6, 957.7, and 605.0 cm^{-1} exhibit constant intensity ratios among themselves and with respect to the 1673.7-, 862.8-, and 765.7-cm^{-1} absorptions; hence, they most probably originate from a single species. Table I exhibits the relative intensities of these bands and the frequencies of their counterparts observed upon reaction of C_3H_4–$^{15}NO_2$ and C_3D_4–NO_2 pairs. As shown in Figure 1b, the most distinct property of this product is that it photodissociates quantitatively upon brief (6 min) 488-nm photolysis at 80 mW cm^{-2}.

In contrast, all remaining product absorptions increase at all photolysis wavelengths, including 488 nm. Comparison of absorbance growth upon irradiation at 580 and 514 nm indicates that these originate from two products whose spectra are given in Tables II and III, including ^{18}O and D data (none of these bands exhibits a ^{15}N isotope frequency shift). Comparison of columns 4 and 5 of Table II shows that this product increases upon 150-min

Table II. Infrared Product Spectrum Assigned to Allene Oxide in a Matrix Allene/NO_2/Ar = 2.5/1/200

frequency, cm^{-1}			absorbance growth of C_3H_4O	
C_3H_4O	$C_3H_4{}^{18}O$[a]	C_3D_4O	A_{580nm}[b]	A_{514nm}[c]
1823.6	1818.4	1767.4	*d*	*d*
		1089.2		
1109.4	1102.3	920.6	0.0056	0.0449
880.0	867.3	745.7	0.0083	0.0640
796.0	794.4	629.3	0.0031	0.0226

[a] Observed in a matrix $N^{16}O_2/N^{16}O^{18}O/N^{18}O_2$ = 2/3/1. [b] Peak absorbance growth upon 580-nm irradiation at 490 mW cm^{-2} for 310 min. [c] Peak absorbance growth upon 514-nm irradiation at 600 mW cm^{-2} for 150 min. [d] Band overlaps with N_2O_4 absorption.

Table III. Infrared Product Spectrum Assigned to Cyclopropanone in a Matrix Allene/NO_2/Ar = 2.5/1/200[a]

frequency, cm^{-1}			absorbance growth of C_3H_4O	
C_3H_4O	$C_3H_4{}^{18}O$[b]	C_3D_4O	A_{580nm}[c]	A_{514nm}[d]
1908.5			0.0069	0.0202
1903.2			0.0043	0.0121
1819.0	1800.0	1840.6	0.0268	0.0752
1045.6	1045.6	1042.6	0.0038	0.0120
966.4	967.2	955.6	0.0035	0.0132
961.4	962.3	953.7	0.0055	0.0073
935.6	934.2	818.7	0.0118	0.0341

[a] Unassigned weak product bands were at 2180.4, 2137.0, and 974.0 cm^{-1} (C_3H_4 + NO_2); 2137.0 and 2110.8 cm^{-1} (C_3H_4 + $N^{18}O_2$); 2144.5, 2137.0, and 974.0 cm^{-1} (C_3H_4 + $^{15}NO_2$); 2177.6, 2144.0, and 2112.0 cm^{-1} (C_3D_4 + NO_2). [b] Observed in a matrix $N^{16}O_2/N^{16}O^{18}O/N^{18}O_2$ = 2/3/1. [c] Peak absorbance growth upon 580-nm irradiation at 490 mW cm^{-2} for 310 min. [d] Peak absorbance growth upon 514-nm irradiation at 600 mW cm^{-2} for 150 min.

514-nm photolysis (600 mW cm^{-2}) 8 times as much as upon 310-min irradiation at 580 nm (490 mW cm^{-2}). According to Table III, the bands of the species displayed there exhibit only a 3-fold difference in absorbance growth in the same two photolysis experiments. This difference furnished the criterion for separating the absorptions of the two species. On the other hand, we have found that at every photolysis wavelength used (585, 580, 552, 537, 514, and 488 nm) all bands listed in Table II grow at constant relative intensities, as do those in Table III. Comparison with matrix infrared spectra of products of the reaction of allene with ozone reported by Singmaster and Pimentel allowed us to assign the species of Tables II and III to allene oxide and cyclopropanone, respectively.[12] An additional band that grows concurrently with allene oxide and cyclopropanone absorbs at 1872 cm^{-1} and is readily assigned to nitric oxide (^{15}NO, 1839 cm^{-1}; $N^{18}O$, 1823 cm^{-1}).

Most revealing regarding identification of the species given in Table I was its secondary photolysis behavior. As shown in Figure 1b, a few minutes of photolysis at 488 nm led to complete loss of all bands of Table I under concurrent formation of allene oxide, cyclopropanone, and NO. Since during such a brief photolysis period with blue light the yield of these final oxidation products from direct photolysis of allene–NO_2 pairs is negligible, we conclude that the species represented by the spectrum of Table I photodissociates to NO and C_3H_4O and therefore has the molecular formula $C_3H_4O_2N$. The two most intense bands at 1674 and 766 cm^{-1} have frequencies and ^{15}N isotope shifts that agree well with N=O and N—O stretching absorptions of previously identified ethyl,[15] 2-butyl,[13,14] isobutyl,[16] cyclopentyl, and cyclohexyl nitrite radicals.[17] This strongly indicates that $C_3H_4O_2N$ is a radical with a nitrite functional group. It exhibits the same long wavelength light induced NO photoelimination that is characteristic for all organic nitrite radicals encountered thus far.[13-17]

1.2. Wavelength Dependence of Photolysis. According to Figure 1, allene oxide, cyclopropanone, and NO are produced by secondary photolysis of nitrite radical C_3H_4ONO. To find out

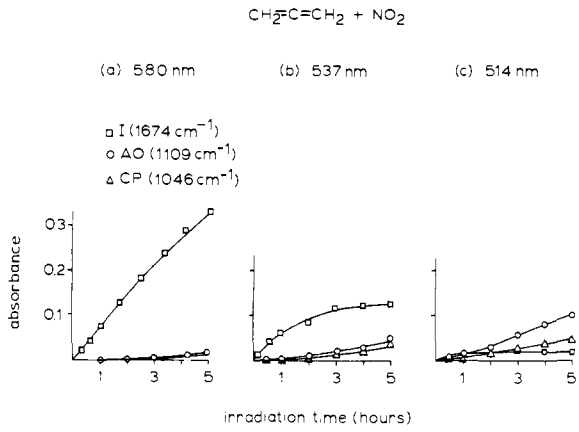

Figure 2. Absorbance growth behavior of nitrite radical at 1674 cm^{-1} (I), allene oxide at 1109 cm^{-1} (AO), and cyclopropanone at 1046 cm^{-1} (CP) upon irradiation of matrices $C_3H_4/NO_2/Ar$ = 2.5/1/100. (a) 580 nm, 500 mW cm^{-2}; (b) 537 nm, 100 mW cm^{-2}; (c) 514 nm, 100 mW cm^{-2}.

Scheme I

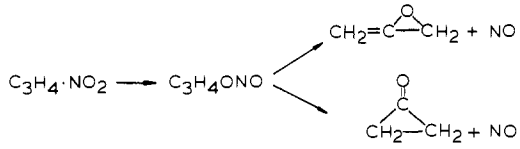

whether the two final oxidation products also emerge from direct, single photon photolysis of allene–NO_2 pairs in addition to photodissociation of accumulated nitrite radical, product absorbance growth curves were measured at various irradiation wavelengths. Figure 2 shows the growth of nitrite radical, allene oxide, and cyclopropanone in matrices allene/NO_2/Ar = 2.5/1/100 at three different photolysis wavelengths, namely 580 (500 mW cm^{-2}), 537 (100 mW cm^{-2}), and 514 nm (100 mW cm^{-2}). Experiments at each wavelength were conducted with a fresh matrix. Since measured infrared bandwidths were found to be constant over the photolysis periods, peak absorbances were used in place of integrated absorbances. While the nitrite radical absorbance growth curves exhibit a single-exponential rise over the initial 2–3-h irradiation at all photolysis wavelengths, both allene oxide and cyclopropanone show an induction period at each wavelength (zero initial slope). Hence, within experimental uncertainty both ketone and epoxide emerge exclusively from secondary photolysis of initially formed C_3H_4ONO. This conclusion is further supported by the good agreement of the calculated (solid) curves of Figure 2 with experimental data points. The former represent fits of integrated rate equations based on a kinetic model that assumes exclusive formation of cyclopropanone and allene oxide by secondary photolysis of C_3H_4ONO, as presented in Scheme I (differential and integrated equations of this model are the same as given in ref 15, eqs 1–8, with k_{3a} = 0). The mathematical treatment and the derivation of the relative reaction quantum efficiencies were described in a previous paper[15] and will not be repeated here. Quantum efficiencies to nitrite radical formation derived from the curve fitting increase by a factor of 1.8 from 580 to 537 nm and by a factor of 2.2 from 580 to 514 nm. Since in the case of the secondary photolysis the extinction coefficient of the reactant, C_3H_4ONO, was not known, only rate constants to allene oxide and cyclopropanone formation (normalized with respect to photolysis laser intensity) could be obtained. However, the two secondary photolysis products originate from the same reactant; hence, the allene oxide/cyclopropanone branching ratio is simply equal to the ratio of the corresponding rate constants. The ratio increases toward shorter photolysis wavelengths, from 1.1 at 580 nm to 1.5 at 537 nm to 2.1 at 514 nm.

2. Dimethylacetylene + NO_2. As in the case of allene + NO_2, no infrared product growth was observed at frequencies above 2200 cm^{-1}; hence, presentation of spectral data will again be limited to the 2200–400-cm^{-1} region. Dimethylacetylene reactant absorptions in solid Ar are at 2057, 1448, 1412, 1407, 1405, 1398, 1379, 1158, 1040, and 1035 cm^{-1}.[23] No distinct reactant pair infrared absorptions were observed.

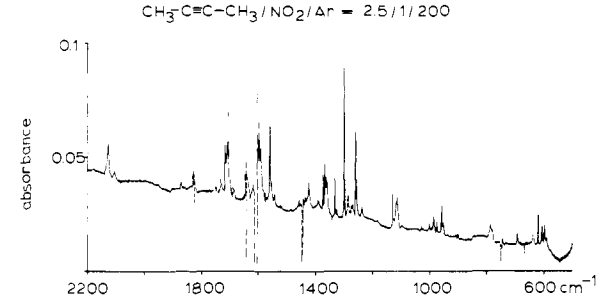

Figure 3. Infrared difference spectrum obtained upon irradiation of a matrix dimethylacetylene/NO_2/Ar = 2.5/1/200 at 585 nm for 3.5 h (350 mW cm^{-2}). Dashed lines indicate N_xO_y and reactant absorptions.

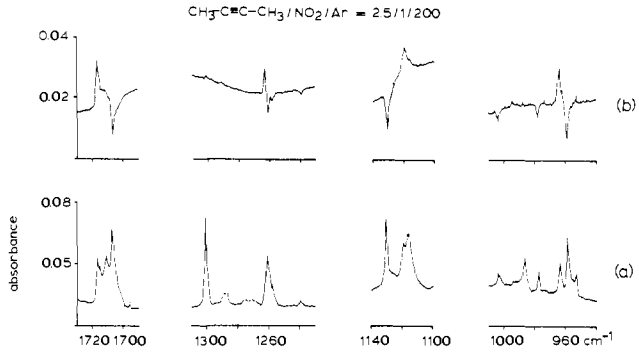

Figure 4. Infrared difference spectra obtained upon 3-min photolysis of a matrix dimethylacetylene/NO_2/Ar = 2.5/1/200 by 514-nm radiation (85 mW cm^{-2}) (b) following product buildup by 3.5-h irradiation at 585 nm (a).

Threshold to reaction of dimethylacetylene–NO_2 pairs was found at 610 nm. Two groups of infrared product bands could readily be assigned to known species, namely a multiplet at 2135.7, 2130.0, 2126.7, and 2104.0 cm^{-1} with an ^{18}O isotope shift of 26.0 cm^{-1}, but no ^{15}N shift, and an absorption at 1872 cm^{-1} with ^{18}O and ^{15}N counterparts at 1823 and 1839 cm^{-1}, respectively. Both the frequency[24] and the ^{18}O isotope shift[25] of the 2100-cm^{-1} absorption are characteristic for the C=O stretching mode of dimethylketene. Since the absorption cross section of the ν(C=O) mode exceeds that of any other infrared absorption by at least 1 order of magnitude, it is not surprising that no other infrared absorption of this product was observed. The 1872-cm^{-1} band is readily assigned to NO. Absorbance growth of both products exhibited single-exponential behavior and linear laser intensity dependence at all photolysis wavelengths used (610, 600, 593, 585, 579, 514, and 488 nm).

As shown in the infrared difference spectrum of Figure 3, a number of additional product absorptions grew in upon irradiation with red light. Many of these absorptions are split into several bands, as can best be seen from the expanded spectra of Figure 4a. Frequencies of these bands, including those of ^{15}N and ^{18}O isotopic modifications observed upon C_4H_6 + $^{15}NO_2$ and C_4H_6 + $N^{18}O_2$ photochemistry with red or yellow light, are given in the first three columns of Table IV. At these photolysis wavelengths all product absorptions given in the table grew according to a single-exponential law and exhibited linear laser power dependence. Absorbance growth upon 200 min of irradiation of a matrix $C_4H_6/NO_2/Ar$ = 2.5/1/200 at 585 nm (350 mW cm^{-2}) is given in column 4 of Table IV. Subsequent brief photolysis at 514 nm (3 min, 85 mW cm^{-2}) allowed us to separate three distinct spectra as can be seen from column 5 of Table IV and from Figure 4b.

(23) Herzberg, G. *Infrared and Raman Spectra*; Van Nostrand: New York, 1945; p 358.
(24) Fletcher, W. H.; Barish, W. B. *Spectrochim. Acta* **1965**, *21*, 1647–61.
(25) Hochstrasser, R.; Wirz, J. *Angew. Chem., Int. Ed. Engl.* **1990**, *29*, 411–3.

Table IV. Infrared Spectrum of Chemically Trapped Transient in a Matrix Dimethylacetylene/NO_2/Ar = 2.5/1/200

frequency, cm^{-1}			absorbance change			
$C_4H_6{}^{16}O_2{}^{14}N$	$C_4H_6O_2{}^{15}N$	$C_4H_6{}^{18}O_2N$[a]	A[b]	A[c]	assignment	mode
1716.7	1715.3	1684	0.0204	0.0146	I_{B1}	
1711.2	1708.8	1681	0.0222	0.0046	I_{B1}, I_{B2}	ν(C=O)
1707.0	1705.4	1677	0.0356	−0.0114	I_A	
(1600)[d]	*d*	(1590)[d]	*d*	*d*	I_{B1}	
1591.4	(1566.6)[d]	*d*	0.0203	0.0009	I_{B2}	
	1544.3				I_A	ν(C=N)
1560.3	1532.2	1546	0.0331	−0.0164	I_A	
1545.3	1523.9	1534	0.0034	−0.0015	I_A	
1436.8	1436.8		0.0031	0.0	I_{B2}	
1429.7	1429.2		0.0038	0.0	I_{B2}	$\delta(CH_3)_{as}$
1425.6	1424.0		0.0102	−0.0022	I_A	
1399.3	1399.7		0.0023	0.0005	I_{B1}	
1394.6			0.0035	−0.0019	I_A	
	1392.8	1391				$\delta(CH_3)_{as}$
1392.4			0.0035	−0.0019	I_A	
1389.1	1389.1		0.0028	0.0	I_{B2}	
1375.1	1374.4	1374	0.0153	0.0127	I_{B1}	
1372.7	1372.0		0.0050	0.0027	I_{B1}	
1368.6	1368.3	1368	0.0204	0.0	I_{B2}	$\delta(CH_3)_s$
1363.4	1363.3	1363	0.0146	0.0	I_{B2}	
1360.3	1359.6	1359	0.0107	−0.0052	I_A	
1335.6[e]	1333.3	1335	0.0055	0.0076	I_{B1}	
1333.2	1328.8	1332	0.0165	−0.0072	I_A	
1328.7	1327.2	1325	0.0029	0.0	I_{B2}	
	1318.8				I_A	$\gamma_r(CH_3)$
1301.0	1294.9		0.0651	0.0017	I_{B2}	ν(N—O)
1261.2[f]	1256.7		0.0365	0.0094	I_{B1}	
1258.0	1258.0		0.0156	−0.0079	I_A	
1239.6	1232.0	1239	0.0041	−0.0020	I_A	
1130.8	1128.5	1128	0.0171	−0.0091	I_A	
1119.7	1120.3	1120	0.0113	0.0060	I_{B1}	$\nu(C—CH_3)_{as}$
1116.1	1115.8	1116	0.0138	0.0012	I_{B2}	
1003.6	1003.2	1003	0.0029	−0.0016	I_A	
993.4	994.0	994	0.0017	0.0013	I_{B1}	
986.5	984.3	982	0.0063	0.0	I_{B2}	ν(C—C)
977.4	972.7	975	0.0040	−0.0022	I_A	$\gamma_r(CH_3)$
963.4	963.2	956	0.0063	0.0056	I_{B1}	
958.8	958.4	955	0.0118	−0.0057	I_A	
953.0	952.7	945	0.0048	0.0012	I_{B1}, I_{B2}	
692.8	689.4	693	0.0048	−0.0030	I_A	$\nu(C—CH_3)_s$
621.6	617.4	616	0.0127	−0.0071	I_A	
608.3	606.2	598	0.0090	0.0076	I_{B1}	
602.5	600.7	593	0.0054	0.0020	I_{B1}, I_{B2}	γ(C=O)$_{op}$, δ(C—C=O), δ(C—N—O)
598.4	594.7	587	0.0102	0.0	I_{B2}	
590.9	590.4	585	0.0044	0.0	I_{B2}	

[a] Matrix $C_4H_6/N^{18}O_2$/Ar = 2.5/1/100. Frequency accuracy was 0.5 cm^{-1} in this experiment. [b] Peak absorbance growth upon 585-nm irradiation at 350 mW cm^{-2} for 200 min (parent isotope). [c] Peak absorbance change upon 3-min irradiation at 514 nm (85 mW cm^{-2}) following product accumulation by 85-nm photolysis for 5 h. [d] Band overlapped by NO_2 absorption. [e] Band overlapped by impurity on CsI window. [f] Band overlapped by absorption of I_A.

One set of bands decreases (labeled I_A), a second set increases (I_{B1}), while intensities of a third set of absorptions with frequencies close to those of the second set remain virtually unchanged (I_{B2}). Classification of all bands according to this behavior is given in the second to last column of Table IV. No growth of dimethylketene or NO was observed during the 3-min irradiation at 514 nm. The fact that bands assigned to I_A, I_{B1}, and I_{B2} are close in frequency and exhibit similar (but not identical) ^{15}N and ^{18}O isotopic shifts strongly suggests that these species are isomers. Only interconversion of species I, but no net loss due to photodissociation, was observed at any photolysis wavelength. Integrated infrared intensity ratios showed that the branching of dimethylketene + NO to I_A + I_{B1} + I_{B2} increased monotonically toward higher photolysis photon energies.

To facilitate assignment of species I_A, I_{B1}, and I_{B2}, infrared spectra of diacetyl monoxime ($CH_3C(=O)C(=NOH)CH_3$) suspended in solid Ar were recorded. A single, sharp OH stretching absorption at 3609 cm^{-1} indicated that the molecule was completely isolated (ν(OH) of intermolecular H-bonded monoxime, by comparison, absorbs in the 3300–3400-cm^{-1} region[26,27]). Figure 5 shows the photolytic changes induced by 3 min of irradiation of diacetyl monoxime at 266 nm (170 mW cm^{-2}).

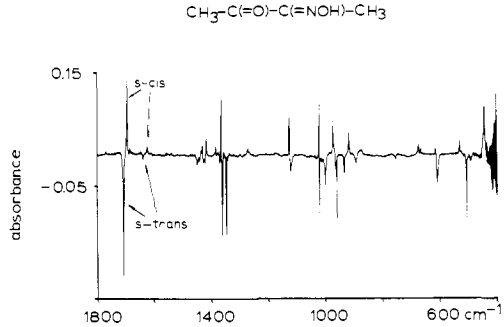

Figure 5. Infrared difference spectrum obtained upon 3-min photolysis of a matrix 2,3-butanedione monoxime/Ar at 266 nm (170 mW cm^{-2}).

IV. Discussion

The trapped intermediates observed both in the allene + NO_2 and in the dimethylacetylene + NO_2 reaction furnish detailed

(26) Hadzi, D.; Premru, L. *Spectrochim. Acta* **1967**, *23A*, 35–44.

(27) Bernadon, J.; Fayet, J. P.; Bonnafons, M.; Mauret, P. *Bull. Soc. Chim. Belg.* **1978**, *87*, 747–52.

Chart I

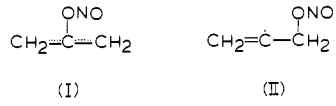

(I) (II)

insight into the reaction paths. We will first discuss the identity of these species on the basis of the infrared data (section 1). In section 2, mechanisms will be proposed for both reactions as inferred from the structures of the trapped intermediates.

1. Identification of Trapped Intermediates. 1.1. Allene + NO_2. Chart I shows the two possible structures of the nitrite radical C_3H_4ONO. Two observations indicate that only one of the two isomers is produced. First, almost all infrared absorptions of the nitrite radical consist of a single band. Second, the product of the observed ^{15}N isotope frequency shifts[28] in the 1700–700-cm^{-1} range (1.036) is equal to the product of the shifts calculated for a ν(N=O) and a ν(N—O) mode which are expected to absorb in this region (1.037, diatomic model). While allene oxide could emerge from ring closure of a transient biradical produced by photoelimination of NO from either nitrite radical I or II, cyclopropanone can only originate from ring closure of the biradical obtained by photodissociation of structure I. Hence, the secondary photolysis behavior strongly suggests that the observed nitrite radical is the allyl nitrite radical I.

Comparison with literature data shows that the infrared spectrum of the nitrite radical is consistent with structure I. Specifically, the high frequency of the ν(N=O) absorption (1674 cm^{-1}) indicates that the conformation about the N—O bond is s-trans as previously observed in the case of alkyl nitrite radicals[13-17] (cis (N—O) conformers of closed shell alkyl nitrites absorb in the 1625–1605-cm^{-1} range).[29,30] Since the observed cumulative ^{15}N shift of the bands in the 1700–700-cm^{-1} region accounts fully for the NO stretching modes (with the 1674- and 766-cm^{-1} absorptions as main contributors), the 3-cm^{-1} ^{15}N shift of the 605-cm^{-1} absorption indicates substantial admixture of another nitrite group mode in the corresponding normal vibration, most probably the O—N=O bending mode. The most suitable guide for empirical assignment of the vibrations of the carbon fragment is the infrared matrix spectrum of allyl radical (CH_2=CH—C$^{\bullet}H_2$) reported by Maier et al.[31] The highest frequency absorption of the carbon fragment in the fingerprint region is at 1429 cm^{-1}, which is typical for CH_2 scissoring modes. Alternative assignment to asymmetric CCC stretching mode (1477 cm^{-1} in the case of allyl radical)[31] is unlikely because C_3D_4ONO does not exhibit a band in this region (Table I). The next two lower infrared absorptions at 1371 and 1335 cm^{-1} are attributed to in- and out-of-phase CH_2 rocking modes, respectively, again using the allyl spectrum as a guide. The 1024-cm^{-1} band is most probably the asymmetric CCC stretching vibration, perhaps drawing intensity from some admixture of ν(C–O). While the 958-cm^{-1} band lies in the region where the CH_2 out-of-phase wagging mode typically absorbs, high intensity and frequency of the 863-cm^{-1} band indicate that this is primarily a C–O stretching mode. Aside from ONO bending contribution, the 605-cm^{-1} absorption is expected to involve to a substantial degree CCO and/or CCC deformation vibrations.

1.2. Dimethylacetylene + NO_2. The observed ^{15}N isotope frequency shifts in the spectra of I_A, I_{B1}, and I_{B2} confirm that these species contain nitrogen. Absorption in the regions 1700–1500 and 1300–1200 cm^{-1} revealed their constitution. Bands at 1717 (I_{B1}), 1711 (I_{B2}), and 1707 cm^{-1} (I_A) have frequencies and ^{18}O isotope shifts (30–33 cm^{-1}) that are indicative of a C=O stretching mode (the calculated shift based on the diatomic oscillator approximation is 41 cm^{-1}). The very small ^{15}N shift of these bands supports this assignment. The absorptions in the 1600–1540-cm^{-1} range have frequencies and ^{15}N isotope shifts (22–28 cm^{-1}) that are characteristic for a C=N stretching vibration[32] (diatomic oscillator shift is 25 cm^{-1}). Although stretching modes of aliphatic nitroso groups also absorb in this region,[33] this possibility is ruled out by the large discrepancy between observed ^{18}O isotope shifts of 10–14 cm^{-1} and the 41-cm^{-1} shift expected for a N=O group. In fact, ν(C=N) modes of C=N—O groups found in nitrones[34] lie closest to our observed frequencies. However, the substantial ^{18}O isotope shift of 10–14 cm^{-1} of the 1600–1540-cm^{-1} bands indicates significant admixture of ν(C=O). Indeed, as the data in Table IV show, the combined ^{18}O shifts of the 1700- and the 1600–1540-cm^{-1} bands account for the entire expected C=O stretching ^{18}O shift of each isomer (in the case of I_A, only one of the bands of the 1560/1545-cm^{-1} doublet is taken into account, as will be explained below). Absorptions of I_A, I_{B1}, and I_{B2} with the next lower ^{15}N isotope effect are at 1301 (I_{B2}, 6.1-cm^{-1} shift), 1261 (I_{B1}, 4.5-cm^{-1} shift), and 1240 cm^{-1} (I_A, 7.6-cm^{-1} shift). Both the frequencies and the high intensities of these absorptions are consistent with assignment to the N—O stretching mode of a C=N—O group.[34] The fact that the observed isotope effects are considerably lower than the 23-cm^{-1} ^{15}N frequency shift calculated for a ν(N—O) mode (diatomic oscillator) signals heavy mixing with other skeletal vibrations. We conclude on the basis of infrared frequencies and isotope shifts of bands in the 1700–1500- and 1300–1200-cm^{-1} regions that the species I_A, I_{B1}, and I_{B2} have a C=O and a C=N—O group.

Chart II

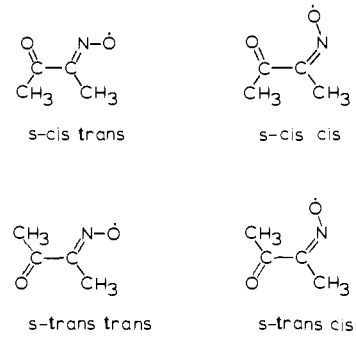

The only constitutional formula we can conceive of that contains these functional groups and is consistent with a species emerging from dimethylacetylene + NO_2 reaction is acetyl methyl iminoxy radical $CH_3C(=O)C(=NO^{\bullet})CH_3$. No vibrational spectra of this or any other iminoxy radical have been reported thus far to our knowledge, but ESR spectroscopic studies of acetyl methyl iminoxy radical in solution are available and suggest that it exists as a mixture of several isomers, namely stable s-trans and unstable s-cis forms (CC bond), each having the additional possibility of cis (syn) and trans (anti) configuration of the iminoxy oxygen.[35] The four isomers are shown in Chart II.

In the light of this isomerism, it is reasonable to interpret I_A, I_{B1}, and I_{B2} spectra in terms of the structures shown in Chart II. Unfortunately, thermodynamic stability in general does not furnish guidance as to conformational branching in the case of species that are produced photochemically in a cryogenic matrix. However, the matrix spectrum of the corresponding (closed shell) oxime, diacetyl monoxime, proved useful since it is known from solid-state infrared spectra[36] and solution NMR measurements[37] that the stable form of the molecule has trans configuration with respect to both the C—C and the C=N bond, as in the trans–trans

(28) Califano, S. *Vibrational States*; Wiley: New York, 1976; p 217.
(29) Tarte, P. *J. Chem. Phys.* **1952**, *20*, 1570–5.
(30) Colthup, N. B.; Daly, L. H.; Wiberley, S. E. *Introduction to Infrared and Raman Spectroscopy*, 3rd ed.; Academic Press: New York, 1990; p 350.
(31) Maier, G.; Reisenauer, H. P.; Rohde, B.; Dehnike, K. *Chem. Ber.* **1983**, *116*, 732–40.
(32) Reference 30, p 344.
(33) Reference 30, p 353.
(34) Hamer, J.; Macaluso, A. *Chem. Rev.* **1964**, *64*, 473–95. Smith, P. A. S.; Robertson, J. E. *J. Am. Chem. Soc.* **1962**, *84*, 1197–1204.
(35) Norman, R. O. C.; Gilbert, B. C. *J. Phys. Chem.* **1967**, *71*, 14–20. Gilbert, B. C.; Gulick, W. M., Jr. *J. Phys. Chem.* **1969**, *73*, 2448–50. Gilbert, B. C.; Norman, R. O. C. *J. Chem. Soc. B* **1966**, 86–91.
(36) Gribov, L. A. *J. Mol. Struct.* **1974**, *22*, 353–60.
(37) Guetté, J. P.; Armand, J.; Lacombe, L. *C. R. Acad. Sci. Paris C* **1967**, *264*, 1509–12.

form of the iminoxy radical (Chart II). Indeed, only two absorptions were observed in the CO and CN double-bond stretching region of diacetyl monoxime suspended in solid Ar, namely an intense band at 1708.4 cm^{-1} (with a weak satellite band at 1712.7 cm^{-1}) and a weak absorption at 1638.9 cm^{-1}. While 1708 cm^{-1} is a typical ν(C=O) frequency, the 1639-cm^{-1} band is in the region where C=N stretching modes of oximes absorb.[32] Following the previous spectroscopic work,[36,37] we assign these bands to the stable s-trans (CC)–trans (CN) stereoisomer of the monoxime (the conformation of the OH group is unknown). As shown in the infrared difference spectrum of Figure 5, brief irradiation of this molecule at 266 nm (3 min, 170 mW cm^{-2}) resulted in loss of the stable conformer and concurrent growth of a new set of bands. A photostationary state was reached after 15 min of photolysis. As can be seen from Figure 5, main peaks of the product in the ν(C=O)/ν(C=N) region are at 1694.3 and 1624.4 cm^{-1}. Several observations strongly suggest that the observed photochemical process is a trans to cis interconversion about the CC bond. First, the intensity ratio of ν(C=O) to ν(C=N) is substantially smaller for the product (11.3) than for the reactant (22.1). Second, the C=O and the C=N stretching bands of the new species are at lower frequency than the corresponding reactant absorptions. Both observations are in agreement with ν(C=O) and ν(C=C) frequency and intensity shifts of α,β-unsaturated carbonyl systems upon trans → cis isomerization, which are caused by the accompanying change in conjugation and vibrational coupling.[38] Although this effect was originally established for α,β-alkenones, it is expected to extend to conjugated C=O/C=N systems as well, especially since ν(C=N) absorbs in the same region as ν(C=C). Third, Figure 5 shows that frequency shifts between reactant and product absorptions are substantial in every region of the spectrum, indicating that the photoinduced interconversion process involves a major structural change of the molecular skeleton. It is therefore unlikely that a mere change of the oxime oxygen position is involved (i.e., trans → cis interconversion about the C=N bond) as this would almost certainly affect the frequency of only a few modes. Instead, it points to a change in the stereochemistry about the central CC bond which is expected to influence most of the modes, in particular those involving the skeleton. Hence, we assign the 266-nm-induced photochemical process of diacetyl monoxime to trans → cis (CC) isomerization.

Comparison of s-cis and s-trans diacetyl monoxime spectra (Figure 5) with those of the iminoxy radical isomers (Figures 3 and 4; Table IV) reveals striking similarities between bands assigned to *cis*-diacetyl monoxime and I_A on the one hand, and, on the other, between *trans*-diacetyl monoxime and the closely spaced bands of I_{B1} and I_{B2}. Similarities are most pronounced in the ν(C=O) and ν(C=N) region and the ranges 1150–1100 and 700–550 cm^{-1}, where I_A and I_B bands exhibit the same pattern (sequence) as those of *s-cis* and *s-trans*-diacetyl monoxime, respectively. Since modes in these regions involve predominantly the $CH_3C(=O)C(=N)CH_3$ frame (see below), this suggests structural similarity of iminoxy radical and oxime skeleton, i.e., that I_A has cis and I_B trans conformation about the CC bond. This assignment is further supported by the fact that at the 514-nm threshold to photoisomerization the iminoxy radical I_A converts to I_B and not vice versa. It is well established that cis conformers of α,β-unsaturated alkenones[39] and 1,3-alkadienes[40] absorb at longer wavelengths than their trans counterparts. We conclude that the analogy between photochemical behavior of iminoxy radical and UV spectral properties of α,β-unsaturated systems and, in particular, the close similarity between the iminoxy radical and diacetyl monoxime infrared spectra suggest that I_A has cis and I_B trans conformation about the CC bond.

Two observations indicate that the I_A bands originate from two distinct isomers. First, the I_A spectrum contains closely spaced absorptions that have significantly different ^{15}N and ^{18}O isotope shifts, indicating that these are not site splittings. Examples are the doublet at 1560.3 (^{15}N shift of 28.1 cm^{-1}) and 1545.3 cm^{-1} (21.4 cm^{-1}) and the doublet at 1258.0 (0 cm^{-1}) and 1239.6 cm^{-1} (7.6 cm^{-1}). Second, the cumulative ^{15}N isotope frequency shift[28] of I_A bands in the 1500–400-cm^{-1} range is 1.032, which is about twice as large as the 1.013 shift of I_{B1} absorptions or the 1.016 shift of the I_{B2} bands in that region (1.018 is the $\nu(^{15}N–O)$ shift predicted by the diatomic oscillator model). The most likely origin of the isomerism of I_A is cis and trans position of the iminoxy oxygen (Chart II). Assuming equal extinction coefficients for the ν(C=N) absorptions at 1560 and 1545 cm^{-1}, the 10 times higher intensity of the 1560-cm^{-1} band would imply that one isomer (I_{A1}) is far more abundant than the other (I_{A2}). This would furnish an explanation for the predominant growth of I_{B1} upon 514-nm-induced $I_A \rightarrow I_B$ interconversion if we further assume that the cis → trans (CC) rotation is not accompanied by a change of the configuration about the C=N bond, i.e., if $I_{A1} \rightarrow I_{B1}$ and $I_{A2} \rightarrow I_{B2}$ (indices 1 and 2 referring to a specific position of the iminoxy oxygen (cis or trans)). While there is good support for the assignment of s-cis and s-trans (CC) conformation to the I_A and I_B forms, respectively, specific assignment of the configuration with respect to the C=N bond cannot be made on the basis of the present data.

Empirical vibrational mode assignment for iminoxy radical bands in the 1500–400-cm^{-1} region is given in the last column of Table IV. It is based primarily on comparison with the vibrational spectrum of biacetyl.[41] Noteworthy is the fact that the symmetric $C–CH_3$ stretching mode at 693 cm^{-1} is observed for I_A and *cis*-diacetyl monoxime but not for I_B and *trans*-monoxime. This is consistent with the pseudocentral symmetry of the s-trans $CH_3C(=O)C(=N)CH_3$ frame and further supports assignment of I_A and I_B to s-cis and s-trans (CC) conformers, respectively.

2. Reaction Mechanism. We have previously established that the mechanism of long wavelength visible light induced reaction of alkene–NO_2 collisional pairs in a cryogenic matrix involves direct O-atom transfer to the CC double bond to form a transient oxirane biradical.[13–18] The observed products indicate that the biradical is stabilized by two processes that compete on an ultrashort time scale, namely ring closure to form epoxide (and/or 1,2-H-migration to yield aldehyde in the case of unconjugated terminal C=C bonds), and combination with concurrently generated NO cage neighbor to give an alkyl nitrite radical. Thus, the observed alkyl nitrite radical constitutes a chemically trapped oxirane biradical. Crucial evidence for intermediacy of an oxirane biradical and hence the direct O-atom transfer mechanism was the observed correlation between the stereochemistry of the carbon skeleton of alkyl nitrite radical and epoxide in the *cis*- and *trans*-2-butene + NO_2 reaction, which at the same time showed that the transient biradical was trapped by NO in its nascent conformation.[13,14] Although product branching from a vibrationally hot (≈45 kcal mol^{-1}) alkyl nitrite radical which might be formed by electrophilic addition of NO_2 to the C=C bond would also account for the concerted behavior of epoxide and nitrite radical stereochemistry, the high degree of stereochemical retention, particularly in the *cis*- and *trans*-CHD=CHD + NO_2 reaction is inconsistent with such a mechanism.[15] The result reported here that the red-light-induced reaction of NO_2–alkyne collisional pairs does not yield a nitrite radical but an iminoxy radical instead definitively rules out the electrophilic NO_2 addition path. It constitutes compelling evidence that the observed radical is formed by NO trapping of a transient biradical and that therefore the primary elementary step of vibronically induced reaction of NO_2–unsaturated hydrocarbon pairs is direct O-atom transfer from NO_2 to the CC multiple bond. We will discuss the structure of the observed nitrite and iminoxy radicals and the photolysis wavelength dependence of the allene + NO_2 and di-

(38) Erskine, R. L.; Waight, E. S. *J. Chem. Soc.* **1960**, 3425–31. Taylor, P. J. *Spectrochim. Acta* **1976**, *32A*, 1471–6. Noack, K. *Spectrochim. Acta* **1962**, *18*, 1625–8. Noack, K.; Jones, R. N. *Can. J. Chem.* **1961**, *39*, 2200–13.

(39) Alves, A. C. P.; Christoffersen, J.; Hollas, J. M. *Mol. Phys.* **1971**, *20*, 625–44. Mecke, R.; Noack, K. *Spectrochim. Acta* **1958**, *12*, 391–3.

(40) Squillacote, M. E.; Sheridan, R. S.; Chapman, O. L.; Anet, F. A. L. *J. Am. Chem. Soc.* **1979**, *101*, 3657–9. Allinger, N. L.; Miller, M. A. *J. Am. Chem. Soc.* **1964**, *86*, 2811–9.

(41) Durig, J. R.; Hannum, S. E.; Brown, S. C. *J. Phys. Chem.* **1971**, *75*, 1946–56.

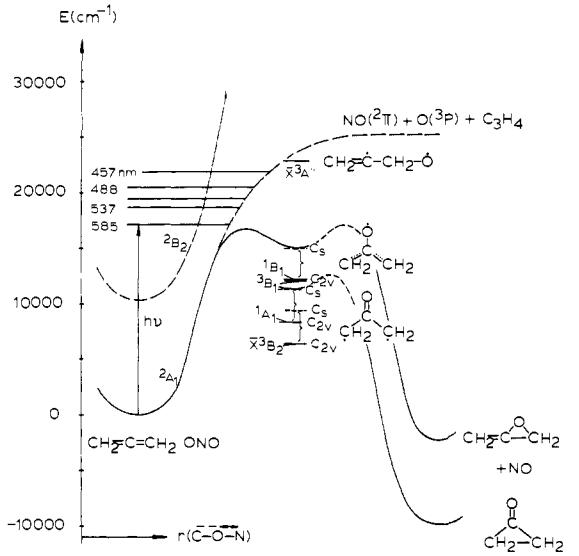

Figure 6. Potential energy diagram for the allene + NO_2 reaction pathway. C_s, twisted conformation; C_{2v}, planar conformation.

methylacetylene + NO_2 systems in terms of electronic states of transient biradicals that may be involved along the respective reaction paths.

2.1. Allene + NO_2. A potential energy diagram for the O-atom transfer path of the allene + NO_2 reaction is presented in Figure 6. Exothermicities for allene + NO_2 → cyclopropanone + NO of −28.4 kcal mol^{-1} and allene + NO_2 → allene oxide + NO of −6.4 kcal mol^{-1} were determined from known standard enthalpies of formation for allene, NO_2, NO,[42,43] and cyclopropanone[44] and from a theoretical estimate in the case of allene oxide.[45] $\Delta H°$ of allene + NO_2 → CH_2=C(ONO)C•H_2 was estimated at −20 kcal mol^{-1} using the calculation method described in the Appendix of ref 13 (taking into account an allyl stabilization energy of 14 kcal mol^{-1}).[46] Electronic ground-state energies of allenylidoxy biradicals C•H_2COC•H_2 and CH_2=C•CH_2O•, species that are expected to be produced upon central and end atom transfer, respectively, were taken from ab initio results of Lester and co-workers.[11] Using these results to estimate reaction enthalpies, $\Delta H°$ = +18 kcal mol^{-1} is obtained for C_3H_4 + $NO_2(\tilde{X}^2A_1)$ → C•H_2COC•$H_2(\tilde{X}^3B_2)$ + $NO(\tilde{X}^2\pi)$ in the case of the stable, planar conformation of the 2-allenylidoxy biradical (C_{2v} symmetry) and +27 kcal mol^{-1} for twisted ground-state conformer (C_s symmetry). Both are indicated in the energy diagram (Figure 6). Endothermicity in the case of end atom attack to yield 1-allenylidoxy biradical CH_2=C•CH_2O•($\tilde{X}^3A''$) is much higher, namely +39 kcal mol^{-1}. The higher energy of CH_2=C•CH_2O•($\tilde{X}$) relative to C•H_2COC•$H_2(\tilde{X})$ originates from the inability of the 1-allenylidoxy biradical to form a CO double bond.[11]

Ab initio results of Morokuma and co-workers indicate that the 2-allenylidoxy biradical CH_2COCH_2 has four low-lying excited states, namely a $^1A_1$ state 5.6 kcal mol^{-1} above the $^3B_2$ ground state, closely spaced singlet and triplet B_1 states 16 kcal mol^{-1} above $\tilde{X}^3B_2$, and a $^1B_2$ state at +26 kcal mol^{-1} relative to the ground state.[47] The lowest three excited states are included in the energy diagram (Figure 6), with energies given for both the stable planar C_{2v} and the unstable, twisted C_s conformation (assuming the 8.5-kcal energy difference between the two forms calculated for the ground state[11] holds for all states, which is certainly an oversimplification). C_s is the nascent conformation of the biradical if we assume that upon O-atom transfer to allene the dihedral angle of the CH_2 groups remains unchanged. The $^3B_2$ and $^1A_1$ states on the one hand and, on the other, the singlet and triplet B_1 states differ in electron orbital occupancy. The $^3B_2$ and $^1A_1$ states have a CO double bond and a lone electron on each methylene carbon (C•H_2C(=O)C•H_2). In contrast, the higher lying $^1B_1$ and $^3B_1$ states have a singly occupied O orbital and an allyl system (CH_2=C(O•)C•H_2 ↔ C•H_2C(O•)=CH_2).

Scheme II

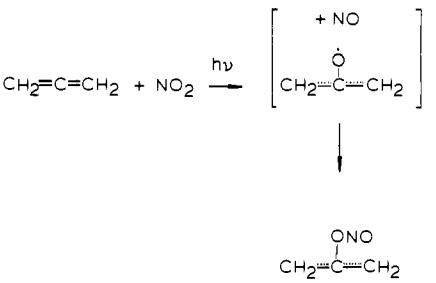

The fact that no nitrite radical CH_2=C•CH_2ONO is observed and hence, by implication, no CH_2=C•CH_2O• produced can readily be explained on energetic grounds. The diagram in Figure 6 shows that even at 488 nm, the shortest photolysis wavelength used to excite allene–NO_2 pairs, photons do not furnish sufficient energy to reach the ground-state 1-allenylidoxy biradical. Hence, the complete regioselectivity signaled by the observed exclusive O-atom attack on the central carbon can be fully explained on the basis of the energetics of the primary photoproduct.

Revealing in terms of the nascent electronic state of 2-allenylidoxy biradical produced upon O-atom transfer to the central carbon is the fact that nitrite, but no nitroso radical, was detected experimentally. Since $^3B_2$ ground and $^1A_1$ excited state biradicals are dominated by an electron configuration that has singly occupied orbitals on carbon but not on oxygen, combination with NO is expected to yield a nitroso radical if 2-allenylidoxy biradical were trapped in one of these two states. In contrast, the higher lying $^1B_1$ and $^3B_1$ biradical states have a singly occupied oxygen p orbital and hence are expected to yield nitrite radical upon combination with NO, as shown in Scheme II (that NO combination at the allyl system to form a nitroso C–N bond is not competitive with N–O bond formation is consistent with our results in the case of NO_2 + alkene photochemistry[13-17]). We conclude that the structure of the observed nitrite radical indicates that O-atom transfer from NO_2 to allene yields 2-allenylidoxy biradical most probably in the singlet or triplet B_1 excited state (both are allowed under the conservation of spin principle), which would imply that combination with NO to form nitrite radical is fast on the time scale of internal conversion or intersystem crossing to the lower lying $^1A_1$ or $^3B_2$ states. Assuming N—O···C=C=C as the reaction plane as a basis for establishing electronic state correlations (Salem diagram),[48] one finds that reaction of ground-state $NO_2(^2A_1)$–$C_3H_4(S_0)$ pairs to yield $CH_2COCH_2(B_1)$ + $NO(^2\pi)$ involves the same type of strongly avoided crossing already discussed in the case of NO_2 + C_2H_4.[15] Correlations of the $^2A_1$ state are relevant here because NO_2 excited at visible wavelengths is a highly vibrationally excited species with mixed $^2B_2$–$^2A_1$ electronic parentage, with the latter dominating strongly.[49] In contrast, under the assumption of the same reaction plane no correlation exists between ground-state reactants and $CH_2COCH_2(\tilde{X}^3B_2$ or $^1A_1)$ + $NO(^2\pi)$, consistent with the lack of formation of nitroso radical.

If the biradical state energies taken from the literature are correct, our conclusion that $^1B_1$ or $^3B_1$ is the nascent biradical electronic state is indeed consistent with the observed 585-nm threshold to reaction. As can be seen from Figure 6, both the

(42) Benson, S. W. *Thermochemical Kinetics*; Wiley: New York. 1968.
(43) Pedley, J. B.; Naylor, R. D.; Kirby, S. P. *Thermochemical Data of Organic Compounds*, 2nd ed.; Chapman and Hall: London, 1986.
(44) Rodriguez, H. J.; Chang, J.-C.; Thomas, T. F. *J. Am. Chem. Soc.* **1976**, *98*, 2027–34.
(45) Kikuchi, O.; Nagata, H.; Morihashi, K. *J. Mol. Struct.* **1985**, *124*, 261–8.
(46) Korth, H. G.; Trill, H.; Sustmann, R. *J. Am. Chem. Soc.* **1981**, *103*, 4483–9.
(47) Osamura, Y.; Borden, W. T.; Morokuma, K. *J. Am. Chem. Soc.* **1984**, *106*, 5112–5.
(48) Salem, L. *Electrons in Chemical Reactions: First Principles*; Wiley: New York, 1982; p 136.
(49) Hsu, D. K.; Monts, D. L.; Zare, R. N. *Spectral Atlas of Nitrogen Dioxide*; Academic Press: New York, 1978.

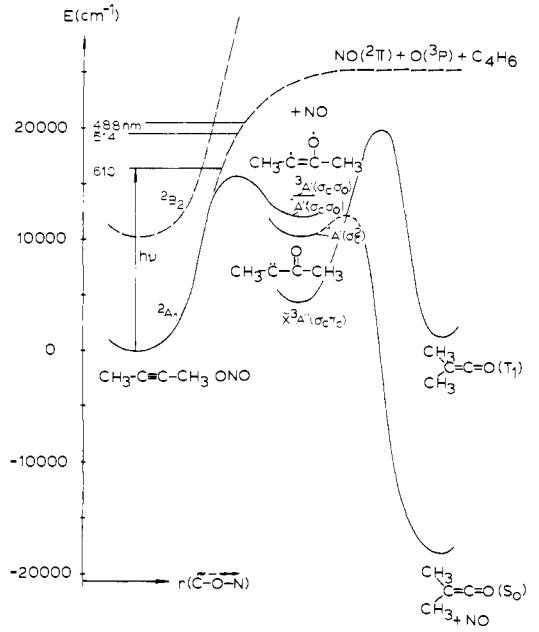

Figure 7. Potential energy diagram for the dimethylacetylene + NO_2 reaction pathway.

$^1A_1$ and the $^3B_2$ state would be accessible energetically by photolysis with light deep in the near infrared (NO_2 absorbs at wavelengths as long as 1000 nm[49]), yet no reaction is observed at these photon energies. The biradical is expected to emerge from the large amplitude O atom transfer from highly vibrationally excited NO_2 in the unstable, twisted C_s conformation which would be suitable for ring closure if $^1B_1$ is the nascent state. The fact that no allene oxide is formed upon direct (single photon) excitation of NO_2–allene pairs at any visible wavelength can readily be rationalized by fast conformational relaxation of initially formed twisted (C_s) B_1 biradical to the stable planar (C_{2v}) conformer, followed by trapping by NO. If the $^3B_1$ state were initially formed, an additional impediment to ring closure would be intersystem crossing to the $^1B_1$ state.

The different electron configurations of biradical $^3B_2$ and $^1A_1$ states on the one hand and, on the other, the $^1B_1$ and $^3B_1$ states also furnish an explanation for the increase of the allene oxide/cyclopropanone branching ratio with increasing photon energy upon allyl nitrite radical photolysis. Absorption of a photon into the nitrite radical charge-transfer absorption[50] results in formation of NO and CH_2COCH_2 biradical. Increase of photolysis photon energy enhances the probability of populating the higher energy $^1B_1$ state (correlating with allene oxide) relative to the lower lying $^1A_1$ state (correlating with cyclopropanone).

2.2. Dimethylacetylene + NO_2. A potential energy diagram showing low-lying states of primary biradical and final product of O-atom transfer from NO_2 to alkyne is presented in Figure 7. For $\Delta H°$ of dimethylacetylene + NO_2 → dimethylketene + NO the exothermicity of the parent reaction NO_2 + HC≡CH → CH_2=C=O + NO of −51.9 kcal mol^{-1} was used. The latter was calculated from known standard enthalpies of formation.[42,51] The energy of the lowest triplet state of dimethylketene given in Figure 7 corresponds to that of CH_2=C=O(^{3}A″) taken from ab initio work by Allen and Schaefer.[52] The enthalpy of reaction to yield electronic ground state biradical, $NO_2(^2A_1)$ + CH_3C≡CCH_3 → $CH_3C^{\bullet}{}^2C(O)CH_3(\tilde{X})$ + $NO(^2\pi)$ was calculated as ΔH = +12 kcal mol^{-1} based on the best estimate for ΔH of $O(^3P)$ + HC≡CH → $HC^{\bullet}{}^2C(=O)H(\tilde{X}^3A''(\sigma_c\pi_c))$ given by Harding.[7]

Also indicated in Figure 7 are the lowest three excited electronic states of the biradical $CH_3CC(O)CH_3$. Energies are approximated by ab initio calculated energies of the HCC(O)H analogue by

Scheme III

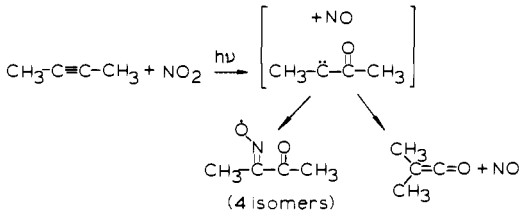

Harding[7] and Bargon and Yoshimine.[53] All calculations agree that the ground state is a triplet state with $A''(\sigma_c\pi_c)$ symmetry. Symmetry designations of formylmethylene states can also be used to characterize corresponding $CH_3CC(O)CH_3$ states if they refer to the plane of the heavy atom skeleton. Symbols in parentheses indicate orbitals occupied by nonbonding electrons. σ means in-plane (sp^2); π stands for perpendicular (p) orbital with respect to the CC(O) plane. Hence, the triplet ground-state biradical has a ketocarbene structure with a CO double bond, a central CC single bond, and a carbene C atom analogous to ground-state vinyl methylene.[54,55] The first excited state of the biradical is a singlet state that has also a ketocarbene electron configuration but with both nonbonding electrons in the sp^2 orbital of the methylene carbon. In the case of HCC(O)H this $^1A'(\sigma_c^2)$ state is situated 17 kcal mol^{-1} above the $^3A''(\sigma_c\pi_c)$ ground state.[53] According to semiempirical calculations by Bachmann et al.[56] the energy difference between the lowest singlet states of $CH_3C^{\bullet}{}^2C(=O)CH_3$ and $HC^{\bullet}{}^2C(=O)H$ would be 4.5 kcal mol^{-1}, which is within the uncertainty of the best ΔH estimate of formylmethylene[7] used in Figure 7. In contrast to these two lowest states, the two next higher states of the biradical that are energetically accessible in our experiment have an electron configuration corresponding to a 1,3-biradical ($CH_3C^{\bullet}$=C(O$^{\bullet}$)CH_3). The $^1A'(\sigma_c\sigma_0)$ state of formylmethylene lies at most a few kilocalories above the $^1A'(\sigma_c^2)$ state,[53] while the corresponding triplet state $^3A'(\sigma_c\sigma_0)$ is situated 27 kcal mol^{-1} above the $^3A''(\sigma_c\pi_c)$ ground state.[7] These energies are used in Figure 7 as estimates for those of corresponding $CH_3CC(O)CH_3$ biradical states.

Interpretation of the concurrent production of iminoxy radical and dimethylketene in the context of these lowest biradical states allows us to propose a detailed path for (single) photon-induced O-atom transfer from NO_2 to dimethylacetylene. According to ab initio work on HCC(O)H,[7,53] barriers to 1,2-migration from the triplet states $^3A'(\sigma_c\sigma_0)$ and $\tilde{X}^3A''(\sigma_c\pi_c)$ are far too high to be accessible in our experiment (the ketocarbene–ketene rearrangement barrier for $^3A''(\sigma_c\pi_c)$ is shown in Figure 7). In fact, Wolff rearrangement of the transient in the presence of the NO cage neighbor is expected to occur only in a state with a very low barrier to 1,2-shift. All ab initio calculations on the parent HCC(O)H system[53,57] indicate that the lowest energy path from the $^1A'(\sigma_c\sigma_0)$ state to ketene proceeds through the $^1A'(\sigma_c^2)$ ketocarbene state; hence, $^1A'(\sigma_c^2)$ is the most likely state in which 1,2-CH_3 group migration takes place.

Electronic structure and conformational distribution of the iminoxy radical give guidance as to the state in which transient $CH_3CC(O)CH_3$ is trapped by NO. Exclusive formation of iminoxy radical (no radical with a nitrite (ONO) functional group is observed) makes it unlikely that the biradical combines with NO while residing in the 1,3-biradical state. This is based on our observation in the allene + NO_2 (section 2.1) and alkene + NO_2 studies[13-17] that NO always combines with O and not with C if

(50) Fitzmaurice, D. J.; Frei, H. Unpublished results.
(51) Nuttall, R. L.; Laufer, A. H.; Kilday, M. V. *J. Chem. Thermodyn.* **1971**, *3*, 167–74.
(52) Allen, W. G.; Schaefer, H. F. *J. Chem. Phys.* **1988**, *89*, 329–44.
(53) Bargon, J.; Tanaka, K.; Yoshimine, M. *Computational Methods in Chemistry*; Bargon, J., Ed.; Plenum: New York, 1980; pp 239–75. Tanaka, K.; Yoshimine, M. *J. Am. Chem. Soc.* **1980**, *102*, 7655–62.
(54) Davis, J. H.; Goddard, W. A.; Bergman, R. G. *J. Am. Chem. Soc.* **1976**, *98*, 4015–7.
(55) Reference 48, p 84.
(56) Bachmann, C.; N'Guessan, T. Y.; Debu, F.; Monnier, M.; Pourcin, J.; Aycard, J.-P.; Bodot, H. *J. Am. Chem. Soc.* **1990**, *112*, 7488–97. Debu, F.; Monnier, M.; Verlaque, P.; Davidovics, G.; Pourcin, J.; Bodot, H.; Aycard, J. P. *C. R. Acad. Sci. Paris Ser. 2* **1986**, *303*, 897–902.
(57) Bouma, W. J.; Nobes, R. H.; Radom, L.; Woodward, C. E. *J. Org. Chem.* **1982**, *47*, 1869–75.

it has the opportunity to select between an O and a C radical center (CH_2=C(O•)C•H_2, C•H_2CH_2O•). Reaction at the C radical center in the case of CH_3C•=C(O•)CH_3 would be more favorable compared to the alkene and allene case because the resulting nitroso radical could rearrange to iminoxy radical, which is more stable than the nitrite radical CH_3C•=C(ONO)CH_3 that would result from combination of NO at the oxygen center. However, the iminoxy radical formed by NO trapping of a $CH_3CC(O)CH_3$ 1,3-biradical state is expected to yield predominantly the s-cis form (I_A), contrary to what we observe. It is more likely therefore that reaction with NO occurs in a ketocarbene state. Since 1,2-CH_3 migration can only take place in the singlet but not in the triplet ketocarbene state, we conclude that $^1A'(\sigma_c^2)$ is the most probable state in which branching between CH_3 group shift and combination with NO cage neighbor occurs (Scheme III). This is consistent with the observed iminoxy radical conformer ratio I_A/I_B of approximately 1 since in the equilibrium structure of the $^1A'(\sigma_c^2)$ state the C•^{2}H(C•$^2CH_3$) bond is approximately perpendicular to the CCO plane according to ab initio work on HC•^{2}C(O)H[53,57] and semiempirical calculations on CH_3C•^{2}C(O)CH_3.[56] Upon CN bond formation the CH_3C(=NO) group would have about equal opportunity to flip either way to yield s-cis or s-trans (CC) radical, giving similar yields of I_A and I_B. The distribution between I_{B1} and I_{B2} (and I_{A1} and I_{A2}) depends presumably on the exact orientation of NO relative to the ketocarbene biradical prior to combination with the carbene C.

On the basis of the dimethylacetylene + NO_2 study alone we cannot rule out the alternative possibility that product branching originates from competition between CH_3 group migration and intersystem crossing of CH_3C•^{2}C(=O)CH_3 ($^1A'(\sigma_c^2)$) followed by NO combination in the $^3A''(\sigma_c\pi_c)$ ground state. This is unlikely, however, in view of results from related studies. First, Bodot, Pourcin, and their groups found recently that the singlet CH_3C•^{2}C(=O)CH_3 products dimethylketene and methyl vinyl ketone observed upon photodissociation of the α-diazoketone $CH_3C(=N_2)C(=O)CH_3$ are diverted to the ketoketene CH_3-C(=C=O)C(=O)CH_3 in CO-doped rare gas matrices.[56] This implies that CO combines with the transient ketocarbene while it resides in the $^1A'(\sigma_c^2)$ state. Since NO is certainly no less efficient than CO in trapping the ketocarbene, there is little doubt that NO reacts with CH_3C•^{2}C(O)CH_3($^1A'(\sigma_c^2)$) prior to intersystem crossing. Second, no iminoxy radical at all is found in the case of visible light induced O transfer from NO_2 to HC≡CH as will be reported in a forthcoming paper[21] (ketene and NO are the sole products). Any triplet ground-state HC•^{2}C(O)H, if formed, would yield iminoxy radical because of the high barrier to 1,2-H shift on the triplet surface. Since none is observed, we conclude that the HC≡CH + NO_2 reaction proceeds exclusively on the singlet HCC(O)H surface. CH_3 group substitution is not expected to affect the intersystem crossing rate; hence, the observed increase of the branching ratio between NO combination and 1,2-migration from HC•^{2}C(O)H to CH_3C•^{2}C(O)CH_3 is most probably due to a change in competition between Wolff rearrangement and NO combination in the $^1A'(\sigma_c^2)$ state.

A Salem diagram[48] shows that $NO_2(^2A_1 - {}^2B_2)$ + CH_3C≡C-$CH_3(S_0)$ does not correlate with $CH_3CC(O)CH_3(^1A'(\sigma_c^2))$ + $NO(^2\pi)$; hence, the state in which competition between CH_3 group migration and combination with NO takes place is not the nascent biradical state. However, correlation exists between reactants and the $^1A'(\sigma_c\sigma_0)$ biradical state, which is expected to be strongly coupled with the $^1A'(\sigma_c^2)$ state because these two states have the same symmetry and are only a few kilocalories per mole apart. The implication is that the $^1A'(\sigma_c\sigma_0)$ state may be extremely short lived. Therefore, the most likely reaction path is O-atom transfer to the CC triple bond to yield $CH_3CC(O)CH_3$ in the $^1A'(\sigma_c\sigma_0)$ state, followed by relaxation to the $^1A'(\sigma_c^2)$ state fast on the time scale of combination with NO.

Triplet ground-state ketocarbenes of larger hydrocarbon systems have been detected by ESR spectroscopy as early as 1966,[58] but infrared and UV spectra of such species have only recently been reported by Chapman and co-workers, who photolyzed diazoketones in rare gas matrices.[59]

It is important to note that we have no evidence for formation of the elusive oxirene CH_3C=C(O)CH_3 despite the fact that it lies on the $^1A'(\sigma_c\sigma_0)$ hypersurface presumed to be accessed upon photolysis of NO_2–dimethylacetylene pairs and that red-light-induced O-atom transfer would produce it with the least amount of excess internal kinetic energy (Figure 7). In their recent work on wavelength-dependent photolysis of α-diazoketone $CH_3C(=N_2)C(=O)CH_3$ in rare gas matrix, Bodot and collaborators[56] have attributed an infrared band at 2137 cm^{-1} (Kr) to dimethyloxirene (2128 cm^{-1} in the case of perdeuterated diazoketone precursor). However, positive identification of dimethyloxirene awaits measurement of ^{13}C and ^{18}O isotope frequency shifts of this absorption because it lies in a spectral region where multiple sites of ketene product absorb (which depend strongly on the method by which the molecule is prepared) and because the ν(C=C) mode is expected to be among the least intense infrared absorptions of oxirene according to recent ab initio infrared intensity calculations on parent HC=C(O)H by Schaefer and co-workers.[60]

V. Conclusions

Biradicals produced upon oxidation of allene and dimethylacetylene by NO_2 excited at long visible wavelengths have been chemically trapped for the first time in a form that reveals the detailed path of O-atom transfer to cumulene and CC triple bonds, respectively. In the case of allene oxidation the result suggests that central atom attack leads to 2-allenylidoxy biradical CH_2=C(O•)C•$H_2(B_1)$ which is trapped as CH_2=C(ONO)C•H_2, while iminoxy radical observed in the case of O-atom transfer to dimethylacetylene indicates formation of ketocarbene CH_3C•^{2}-C(=O)CH_3($^1A'(\sigma_c^2)$) via the strongly coupled CH_3C•= C(O•)CH_3($^1A'(\sigma_c\sigma_0)$) 1,3-biradical state. The latter is ring-opened oxirene, yet no dimethyloxirene was observed. This novel point of entry to singlet $CH_2C(O)CH_2$ and $CH_3CC(O)CH_3$ biradical hypersurfaces opened up by large amplitude O atom transfer from NO_2 may be typical for cumulene and CC triple bond oxidation by common closed shell oxidizers like peroxy acids. It is interesting to compare these cases with O(^{3}P) reactions under single-collision conditions. O(^{3}P) + HC≡CH chemistry proceeds on the triplet ground-state surface throughout, leading to Wolff rearrangement as well as H-atom elimination,[6] while reaction of CH_2=C=CH_2 with O(^{3}P) involves in its initial step branching between triplet ground-state C•$H_2C(O)C$•H_2 and CH_2C•CH_2O• biradical, with the former dominating.[9]

Comparison of the results reported here with those of O-atom transfer from NO_2 to alkenes[13-17] reveals an interesting similarity between the mechanisms of CC double- and triple-bond oxidation. In both cases a biradical intermediate is trapped, a ground-state singlet oxirane biradical in the case of alkene oxidation, a singlet ketocarbene in the case of dimethylacetylene oxidation, the latter presumably preceded by an excited 1,3-biradical state. This indicates that O-atom transfer is asymmetric in both cases, leading to a biradical intermediate rather than oxirane or oxirene through O-atom insertion in a single step.

Acknowledgment. This work was supported by the Director, Office of Energy Research, Office of Basic Energy Sciences, Chemical Sciences Division of the U.S. Department of Energy, under Contract No. DE-AC03-76-SF00098.

Registry No. I, 138151-83-4; NO_2, 10102-44-0; NO, 10102-43-9; H_3CC≡CCH_3, 503-17-3; $H_3CC(CH_3)$=C=O, 598-26-5; $H_3CC(O)C$-(CH_3)=NOH, 57-71-6; $H_3CC(O)C(CH_3)$=N—O•, 138151-84-5; H_2C=C=CH_2, 463-49-0; allene oxide, 40079-14-9; cyclopropanone, 5009-27-8.

(58) Trozzolo, A. M. *Acc. Chem. Res.* **1968**, *1*, 329–35. See refs 4 and 5 for further references.

(59) McMahon, R. J.; Chapman, O. L.; Hayes, R. A.; Hess, T. C.; Krimmer, H.-P. *J. Am. Chem. Soc.* **1985**, *107*, 7597–606.

(60) Vacek, G.; Colegrove, B. T.; Schaefer, H. F. *Chem. Phys. Lett.* **1991**, *177*, 468–70.